

Article

Generating Self-Shaped 2D Aluminum Oxide Nanopowders

Meng-Ying Lee , Fu-Su Yen * and Hsing-I Hsiang 

Department of Resources Engineering, National Cheng Kung University, Tainan 70101, Taiwan

* Correspondence: yfs42041@mail.ncku.edu.tw; Tel.: +886-6-2757575 (ext. 62822)

Abstract: The thermal-assisted exfoliation phenomena of boehmite particles under moderate heating rates were examined. The exfoliation that generated flakes of 5–6 nm in thickness can be achieved because of the perfect cleavage on the boehmite particles that are stripped when thermal treatments bring about dehydration and γ -Al₂O₃ formation in sequential phase transformation of boehmite. Examinations of the exfoliation effects were carried out on calcined boehmite single crystal particles, which were about 500 nm in diameter, and obtained at three heating rates 0.5, 1.0, and 2.0 °C/min with the heating schedules. The TEM techniques, BET-N₂ measurements, XRD-Scherrer equation, and AFM images were employed in the examination. That the BET values increased as increasing of exfoliated flakes reflected two stages of exfoliation. In the beginning stage, during which the BET values were <40 m²/g, the exfoliation resulted from the stress produced by dehydration. In the second stage, the increased rate of surface area was due to the additional force, which originated from the γ -Al₂O₃ formation. Exfoliation occurred on the cleavage planes {010}, the side pinacoid of the boehmite particle. The generation of flakes resulted in the thinning of boehmite particles. Some of the flakes preserved the external form of boehmite crystals. From the surface energy evaluations of boehmite and γ -Al₂O₃, it can be inferred that exfoliation is a natural way of thermal treatment.

Keywords: 2D powders; top-down; layered material; thermal-assisted exfoliation; transition alumina; cleavage; pseudomorph



Citation: Lee, M.-Y.; Yen, F.-S.;

Hsiang, H.-I. Generating Self-Shaped 2D Aluminum Oxide Nanopowders. *Nanomaterials* **2022**, *12*, 2955. <https://doi.org/10.3390/nano12172955>

Academic Editor: Jun Shimizu

Received: 1 August 2022

Accepted: 23 August 2022

Published: 26 August 2022

Publisher's Note: MDPI stays neutral with regard to jurisdictional claims in published maps and institutional affiliations.



Copyright: © 2022 by the authors. Licensee MDPI, Basel, Switzerland. This article is an open access article distributed under the terms and conditions of the Creative Commons Attribution (CC BY) license (<https://creativecommons.org/licenses/by/4.0/>).

1. Introduction

Ultrathin two-dimensional (2D) nanomaterials, with their unique and indispensable high specific surface area [1] and relatively large lateral size, offer some novel physical, chemical, and electronic properties due to their electron confinement in 2D [2]. A wide range of applications was developed, such as electronics/optoelectronics [3,4], catalysis [5,6], and thermal wear coatings [7,8]. The preparation methods of ultrathin 2D nanomaterials can be categorized into top-down and bottom-up two approaches. Top-down approaches were applied to those layered compounds, such as graphene [9–12], h-BN [13–16], and MoS₂ [17–19]. Most of the compounds display good cleavage planes that can be exfoliated using Scotch tape [20] or other microchemical cleavage techniques [21–23], including electrochemical exfoliation [18,24–26] and thermal treatments [10,11,27,28] depending on voltage-driven or released gas between interlayers or sheets followed by expansion and finally exfoliation. It is non-destructive but normally has high technical requirements. Bottom-up approaches have been used to produce inorganic 2D nanomaterials [29], such as transition metal oxides (e.g., TiO₂, ZnO, Co₃O₄) [30] and metal chalcogenides (e.g., PbS, CuS, CuSe, SnSe) [31], etc. CVD techniques [19,32,33] and other wet-chemical synthesis methods [34–36] were adopted. However, these methods are complicated in technique and relatively high cost.

The concept offered in this study is the utilization of autogenous forces originating from thermal treatment so as to break the cleavage planes to produce flakes. The raw material used in this study is an aluminum hydroxide mineral, boehmite, which is a lamellar-structured mineral with the prominent perfect cleavage {010}_b (side pinacoid) on the particles [37]. Boehmite is transformed to γ -Al₂O₃ when the temperature reaches

450 °C and boehmite undergoes a topotactic transformation to another layered oxide, γ -Al₂O₃ [38]. The side pinacoid {010}_b of boehmite and the tetragonal prism {110}_γ of γ -Al₂O₃ are the most relevant crystallographic orientations [39–42], representing the same and preferentially exposed surface on the particle.

The phase transformation to γ -Al₂O₃ provokes the release of structural water and an increase in molar density from 3.07 to 3.71 g/cm³. The former generates water vapor pressure between the cleavage planes [43,44]. The latter results in dimension difference between boehmite and the new-formed γ -Al₂O₃ [45,46], which may trigger displacement on either side of the cleavage planes [47].

Table 1 lists the orientation relationship between boehmite and γ -Al₂O₃ and schematically illustrates the views of cleavage surfaces {010}_b and {110}_γ to emphasize that these two cleavage planes are equivalent. Diffraction data from the powder diffraction file [48] (In text: PDF 21-1307 and PDF 29-0063) were used to simulate the characteristic morphology. If boehmite is converted to γ -Al₂O₃, the axial lengths of a- and c- of boehmite vary by +7.1% and −2.3%, respectively. The interfacial angles constituting the cleavage planes {010}_b and {110}_γ are 75.5° (boehmite{101}∧{101}) and 70.5° (γ -Al₂O₃{111}∧{111}). The dimension difference induces a displacement force on either side of the cleavage planes, resulting in the occurrence of exfoliation.

Table 1. The orientation relationships between boehmite and γ -Al₂O₃.

| Boehmite | | | γ -Al ₂ O ₃ | | Relative Difference |
|----------|--------|---|--|-------|---------------------|
| a | 3.700 | → | 1/2 c _γ | 3.962 | +7.1% |
| b | 12.227 | | 2 d ₁₁₀ | 11.2 | −8.4% |
| c | 2.868 | → | 1/2 d ₁₁₀ | 2.802 | −2.3% |

Bearing this in mind, it is of great importance to offer the concept from this topic that the hydroxide minerals with a laminated structure have the basis for the generation of flake powders. The process does not have complex steps and is environmentally friendly, and the operation method can be further improved to make flake powder with a high specific surface area. In addition to extending the current understanding of boehmite, the results will be applicable to other similar and related systems such as gibbsite [49,50], γ -FeOOH [51], Co(OH)₂ [26,52], and Cd(OH)₂ [53,54].

In this paper, the exfoliation of boehmite under moderate thermal treatment was investigated. Particle size (especially thickness), morphology, and the mechanism of flake formation were also evaluated. The examination was carried out on calcined boehmite single crystal particles with a diameter of about 500 nm at three heating rates of 0.5, 1.0, and 2.0 °C/min at predetermined temperatures using TEM techniques. The thickness of the flakes was estimated by BET-N₂ measurements and XRD-Scherrer equation and finally compared with AFM images.

2. Experimental Procedure

2.1. Material

High purity (>99.9%) boehmite powders, γ -AlO(OH) (Shandong Gemsung Crystal Technology Co., Ltd. Zibo City, China) were used in this study. The as-received powders were de-agglomerated using ball milling in deionized water (solid content of ~30 wt%, pH = 4.0 adjusted by 2N HNO₃) using 3 mm diameter alumina balls. The milled slurry was passed through a 400-mesh standard sieve (<38 μm). After drying in a microwave oven,

the dried powder was thermally treated at predetermined heating schedules to obtain test samples. The basic properties and characteristics of the starting boehmite powders are shown in Table 2 and Figures 1 and 2.

Table 2. Basic properties and characteristics of the starting boehmite powder.

| | | |
|---------------------------|-------------------|----------------------------|
| Specific surface area | m ² /g | 15 |
| D ₅₀ | nm | 450 |
| L.O.I. (loss on ignition) | % | 15 + 2 (physical adsorbed) |

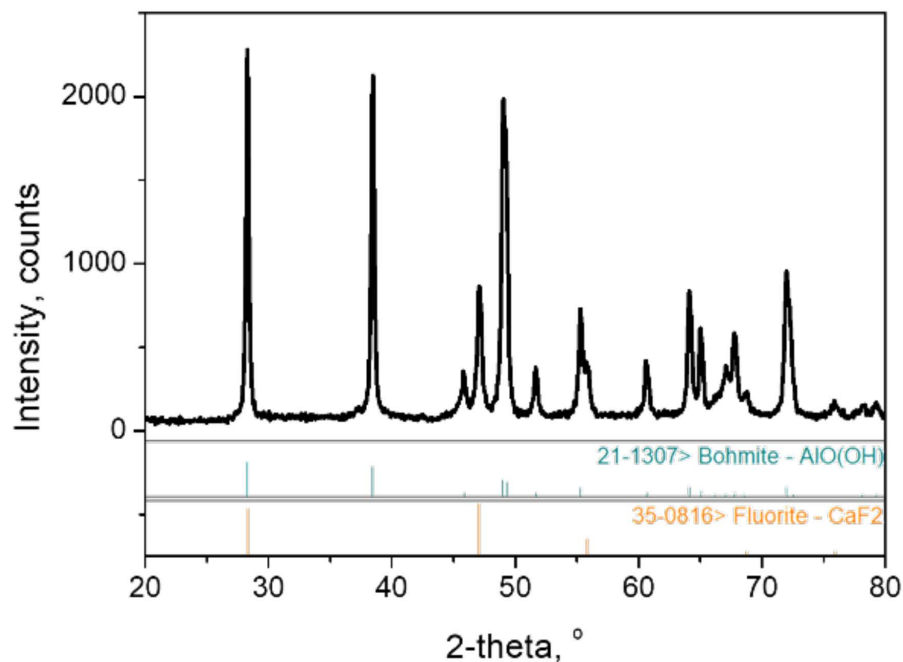


Figure 1. XRD patterns of starting boehmite powders used in this study.

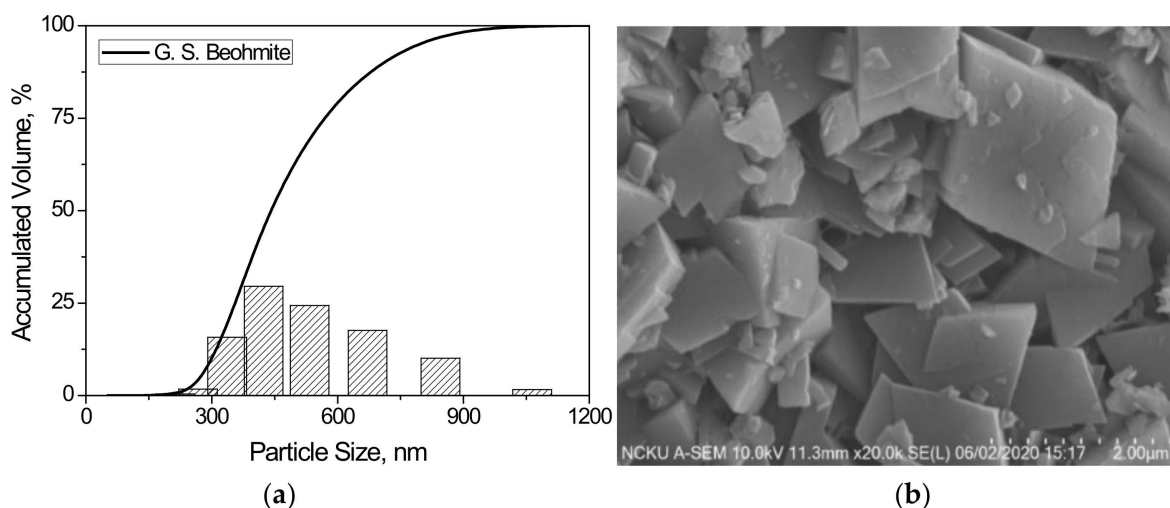


Figure 2. (a) Particle size distribution and (b) SEM micrograph of starting boehmite powders used in this study.

By heating the starting boehmite powders at the heating rates of 0.5 °C/min (450 °C~510 °C), 1.0 °C/min (460 °C~520 °C), and 2.0 °C/min (470 °C~530 °C). The calcined samples (2–3 g each) were collected every 5~10 °C to examine exfoliation effects and the transformation process. The predetermined temperature ranges shown in parentheses were obtained

using the DTA technique under heating rates of 0.5, 1.0, and 2.0 °C/min, respectively. When the set temperature was reached, the sample was removed directly from the furnace and allowed to cool to room temperature (cooling rate > 150 °C/min). Please refer to Appendix A: Figure A1 for the phase transformation under each condition.

2.2. Characterization

The differential thermal analysis (DTA, Labsys evo, Setaram, Lyon, France) technique under the above three heating rates was employed to determine the endothermic temperature ranges induced by dehydration of boehmite and the temperature of boehmite transition to γ -Al₂O₃. The weight losses (%) of samples before and after the thermal treatments were recorded $((W_{\text{before}} - W_{\text{after}}) \times 100\% / W_{\text{before}})$. The fractions of boehmite and γ -Al₂O₃ in the calcined samples were determined by quantitative XRD (Rigaku MiniFlex, Rigaku Corp, Tokyo, Japan) method using Ni-filtered CuK α radiation with CaF₂ (10 wt%) as the internal standard. The integrated intensities of boehmite: (010)_b ($2\theta = 14.45^\circ$), γ -Al₂O₃:(222) _{γ} ($2\theta = 39.36^\circ$), and CaF₂:(111) ($2\theta = 28.27^\circ$) were measured. Their ratios were then compared with the boehmite/ γ -Al₂O₃-CaF₂ calibration curves. The variation of specific surface area values [55] of the powder system was measured by BET (Micromeritics Gemini 2390, Norcross, GA, USA) to identify the exfoliation progress. Morphological investigations including cross-sectional sizes (Feret's diameter [56]) distribution of the calcined samples in each stage were performed by TEM (FEG-TEM, Tecnai G2 F20, FEI, Hillsboro, OR, USA) and AFM (JPK Nanowizard AFM, Axiovert 200, Berlin, Germany) analysis.

In this study, measurements of the thickness of the obtained powders after thermal treatments were carried out in three ways:

1. Mean thicknesses of the calcined boehmite/ γ -Al₂O₃ flakes

The mean thicknesses of calcined boehmite/ γ -Al₂O₃ flakes were derived by measuring the BET-specific surface area values and expressed in terms of t_{BET} . It was assumed that the calcined powder is composed of flake particles with a mean cross-sectional diameter of D (in this case, about 450 nm). The thickness t_{BET} was then calculated by (Equation (1)) (Appendix B, Figure A2).

$$t_{\text{BET}}(\text{nm}) = \frac{2D}{\rho \times D \times \text{BET S.S.A.} \times 10^{-3} - 4} \quad (1)$$

where D : Diameter in average of the cross-sectional area (450 nm)

ρ : Density of boehmite/ γ -Al₂O₃ (g/cm³)

and S.S.A. (Specific surface area): BET specific surface area value (m²/g)

2. Thickness of boehmite and γ -Al₂O₃ flakes

The thickness of boehmite and γ -Al₂O₃ flakes were calculated by the XRD-Scherrer equation [57],

$$D_{\text{hkl}} = \frac{K\lambda}{B\cos\theta} \quad (2)$$

where D_{hkl} is the crystallite size in the direction perpendicular to the lattice planes, K is a numerical factor and is usually taken as about 0.89, λ is the wavelength of the X-rays (Cu K α 1 radiation ((1.540562 Å)), B is the Full width at half maximum (FWHM) in radians, and θ is the Bragg angle. The reflection peaks of boehmite: (020)_b ($2\theta = 14.5^\circ$) and γ -Al₂O₃:(440) _{γ} ($2\theta = 66.7^\circ$) were used in the cleavage directions, and the 2θ of 13.5°–15.5° for boehmite and 64°–70° for γ -Al₂O₃ with a scanning rate of 0.5°/min were applied. The peak widths of the instrument were calibrated with well-crystallized silicon powder. Data calculations were performed with the assistance of software, XRD pattern processing, and identification, Jade for Windows, Version 5.0. The obtained thickness of boehmite and γ -Al₂O₃ flakes are expressed in terms of $t_{\text{B}(010)}$ and $t_{\gamma(110)}$.

3. AFM

Samples were imaged by AFM in intermittent contact mode. The probe was a Tap 150Al-G silicon probe.

3. Results and Discussion

3.1. The Effects of Thermal Treatment on Boehmite

The thermal treatment on boehmite brings about its dehydration and the phase transformation into γ -Al₂O₃. As the heating proceeded, the weight loss was accompanied by an increase in the specific surface area (BET-N₂), which is related to the exfoliation of the calcined boehmite. Figure 3 illustrates the BET values (Figure 3a) and mineral phase changes (Figure 3b) in relation to the weight loss for samples prepared at three heating rates. At the beginning of the thermal treatment, the dehydration induced a 2% weight loss of physically absorbed water; it was then followed by a 13% weight loss of the structural water. Further heating at temperatures above 600 °C resulted in a weight loss of about 2%.

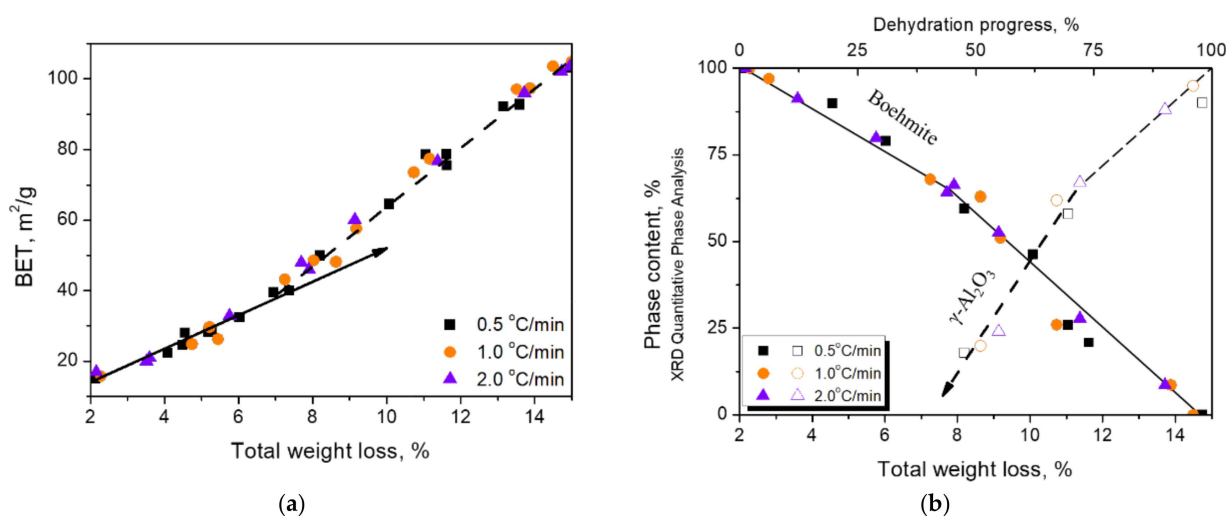


Figure 3. Two stages of BET value increments with the weight loss (a). Correlation between the phase contents of boehmite and γ -Al₂O₃ and weight loss (b).

In Figure 3a, the relationship of specific surface area with the weight loss showed a turning point at 40 m²/g or about 7% of the weight loss, and then the slope became steeper until the specific surface area reached 100 m²/g. Figure 3b shows the disappearance of boehmite and the formation of γ -Al₂O₃ in relation to weight loss. It can be seen that the boehmite content began to decrease when the weight loss reached 2%. However, the formation of γ -Al₂O₃ did not start until the weight loss reached 7% or the BET value reached 40 m²/g, which is comparable to the turning point shown in Figure 3a.

If the increase in BET value is related to the exfoliation of boehmite particles, from the BET value turning point in Figure 3a,b, it is assumed that the surface area increase can be divided into two stages, each of which was dominated by different operating forces. In the beginning, the operating force was mainly contributed by dehydration until the BET value reached 40 m²/g. The increased rate suggested that in the second stage, an additional force was derived from the dimension difference of the cleavage planes due to the presence of γ -Al₂O₃. The exfoliation was first caused by the water vapor pressure generated by the release of structural water of boehmite and was completely controlled solely by water vapor. As the weight loss increased to 7% or the BET value reached 40 m²/g, the dimension difference, which occurred from the phase change to γ -Al₂O₃, added another operating force to the process.

The quantitative phase analysis (Figure 3b) showed that the disappearance of boehmite and the formation of γ -Al₂O₃ did not carry on synchronously during the phase transformation. It can be seen that the γ -Al₂O₃ phase started to appear after nearly 30% of the boehmite disappeared. It is worthwhile to note that this 30% of the boehmite actually

transformed to boehmite-derivative before the appearance of γ - Al_2O_3 , which is characterized by the released or partially released structural water. The boehmite-derivative may be a transition state between structurally collapsed boehmite and structurally established γ - Al_2O_3 [58]. The morphology of the $\{010\}_b$ cleavage plane inherited from boehmite is easily found by TEM (Figure 4). In this study, this derivative is tentatively designated as meta- γ . The meta- γ content decreased with the increase of thermal treatment temperature. When boehmite disappeared completely, the meta- γ content was also close to zero, and γ - Al_2O_3 content was close to 100%.

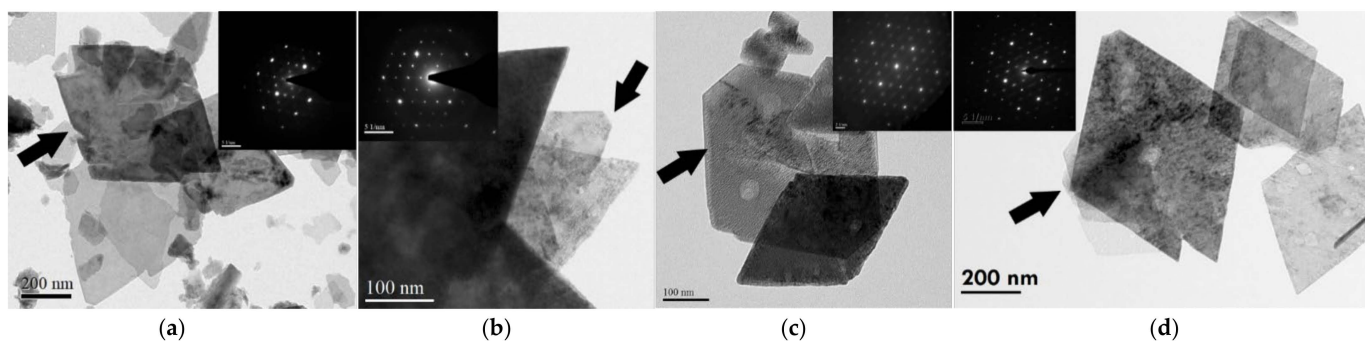


Figure 4. TEM micrographs and diffraction patterns of thermally treated boehmite, (a) boehmite particles, (b) meta- γ particles, (c) γ - Al_2O_3 particles pseudomorph after boehmite, and (d) γ - Al_2O_3 particles.

3.2. The Characteristics of Flakes

3.2.1. Four Types of Flakes Particles

For the calcined samples, four types of lamellar particles can be observed. Figure 4a shows the morphology of boehmite, which was classified as a powder system with a BET value of less than $40 \text{ m}^2/\text{g}$. Figure 4b shows the morphology of meta- γ , which verified that the ratio of d-values (obtained by SAED) in both directions of the cleavage planes lies between boehmite and γ - Al_2O_3 (Table A1). The highest ratio, about 30%, can be found in samples with BET values of around $40 \text{ m}^2/\text{g}$. Figure 4c shows γ - Al_2O_3 particles existed in a pseudomorph form after boehmite. This is usually found in calcined samples with BET values from 40 to $80 \text{ m}^2/\text{g}$. Figure 4d shows the γ - Al_2O_3 flakes per se and the complete structure and morphology. The γ - Al_2O_3 flakes are mainly present in calcined samples with BET values above $80 \text{ m}^2/\text{g}$ (Table A2).

3.2.2. The Thickness Evolution of Particles

Figure 4 shows the average thickness t_{BET} , which was calculated by Equation (1), as well as the BET values of the calcined boehmite. The same figure also shows the thickness of boehmite, $t_{\text{B}\{010\}}$, γ - Al_2O_3 , $t_{\gamma\{110\}}$, and meta- γ , $t_{\text{meta}(\text{BET})}$ in the calcined samples at the corresponding BET values. The thickness $t_{\text{B}\{010\}}$ and $t_{\gamma\{110\}}$ were calculated by the XRD-Scherrer equation (Equation (2)), and $t_{\text{meta}(\text{BET})}$ was calculated by Equation (1) based on the phase content ratios and the thickness of coexisting boehmite and γ - Al_2O_3 . According to the results, $t_{\text{meta}(\text{BET})}$ has an average value of $\sim 6 \text{ nm}$, which is comparable to the value of $t_{\gamma\{110\}}$. It is worthwhile to mention that the thickness of γ - Al_2O_3 was from 5 to 6 nm after its appearance (estimated by Equation (1) or Equation (2)). Therefore, the thicknesses of γ - Al_2O_3 and meta- γ can be considered equivalent.

From the thickness data shown in Figure 5, it can be deduced that the thinning process of boehmite started from the initial $t_{\text{B}\{010\}}$ values of 55–49 nm before the appearance of γ - Al_2O_3 . After that, the thinning process accelerated until $t_{\text{B}\{010\}}$ reached the final minimum value of 22 nm. While both γ - Al_2O_3 and meta- γ as exfoliated products exhibited almost the same thickness, 5–6 nm, and remained essentially constant throughout the phase transition. Further examination using the AFM technique also confirmed the above results (see Figure 6).

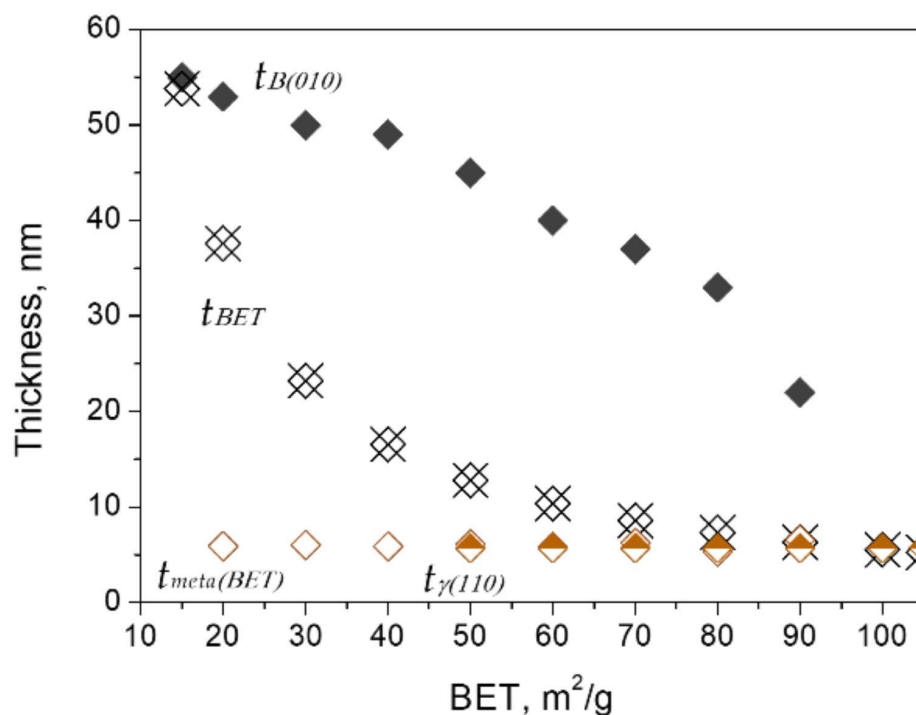


Figure 5. Variations of the average thickness of calcined boehmite samples (t_{BET}) and flakes of boehmite ($t_{B(010)}$), γ -Al₂O₃ ($t_{\gamma(110)}$), and meta- γ ($t_{meta(BET)}$) with exfoliation.

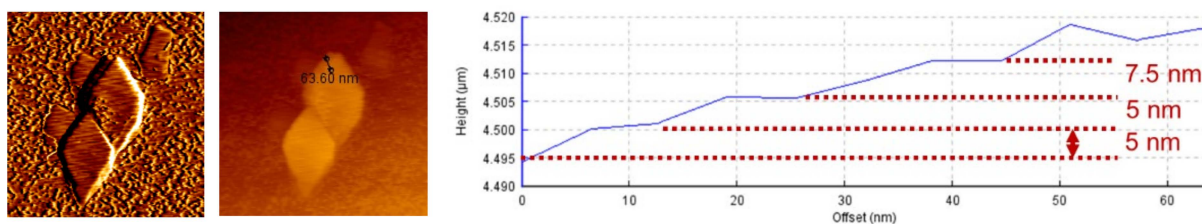


Figure 6. AFM results show the exfoliated flakes displayed approximate thickness of 5 nm.

It is clear that thermal treatments on boehmite can produce exfoliation effects on boehmite particles and bring about an increase in specific surface area (BET values). Table 3 demonstrates the changes of calcined samples in mineral phase content, particle shape ratio, and thickness of flakes for samples of BET values of 40, 70, 90, and 100 m²/g. The exfoliation of boehmite particles, depicted by the BET values, continued as the thermal treatment proceeded. The BET values are contributed by residual boehmite particles and newly formed γ -Al₂O₃ and meta- γ flakes. The boehmite particles gradually became thinner due to exfoliation, and the γ -Al₂O₃ and meta- γ flakes remained at a constant thickness of 5–6 nm. When boehmite was completely transformed, flake powders of γ -Al₂O₃ with a thickness of 5–6 nm were obtained.

Table 3. Property variations of calcined boehmite samples.

| BET, m ² /g | Phase Contents, % | | | Particle Shape, %/Thickness, (nm) | | Pseudomorph (% , est.) | |
|------------------------|-------------------|---|--|-----------------------------------|----------------------|------------------------|----|
| | Boehmite | (Meta- γ)/ γ -Al ₂ O ₃ | γ -Al ₂ O ₃ | Boehmite | Meta- γ | | |
| 40 | 70 | (30)/0 | 0 | 100/(49) ² | –/(5.9) ¹ | 0/(5.8) ¹ | – |
| 70 | 37 | (13)/50 | 50 | 74/(37) ² | –/(6.2) ¹ | 26/(5.7) ² | 48 |
| 90 | 12 | (5)/83 | 83 | 52/(22) ² | –/(6.5) ¹ | 48/(5.7) ² | 42 |
| 100 | 0 | (0)/100 | 100 | 35/– | –/– | 65/(5.7) ² | 35 |

¹: thickness via Equation (1); ²: thickness via Equation (2).

Figure 7 demonstrates that at a moderate heating rate, the thermal treatment to produce exfoliation may begin from small particles. A rough statistical sampling of the number of flakes with different cross-sectional sizes was carried out on TEM images of samples with BET values of 40, 70, and 90 m²/g. It reveals that in the early stage (40 m²/g), exfoliation mainly occurred on small-sized particles, resulting in a high percentage of small flakes. As the BET values increased, i.e., in the later stage, relatively large flakes appeared.

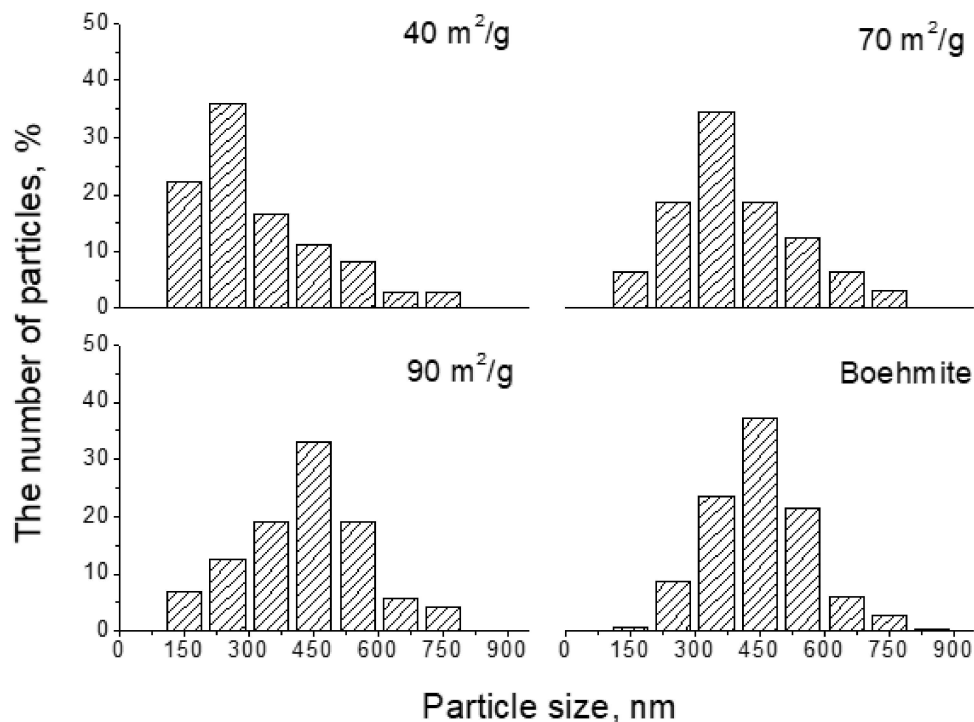


Figure 7. Cross-sectional size distribution of the exfoliated flakes. As the BET value increased, relatively large flakes appeared.

3.2.3. Boehmite Relics in γ -Al₂O₃ Flakes

Because thermal-assisted exfoliation occurs on the cleavage plane {010}_b of boehmite, the generated γ -Al₂O₃ flakes should possess the topotactic nature of boehmite. These γ -Al₂O₃ flakes apparently inherited the morphology or particle shape of boehmite, forming a pseudomorph after boehmite (Figure 4c). Apparently, at higher temperatures, some of the flakes transformed into γ -phase morphology (Figure 4d). Samples with high BET values have the possibility to contain more γ -Al₂O₃ flakes with γ -Al₂O₃ morphology. Detailed examination reveals that the flakes in pseudomorphism decreased from 48 to 42% as the BET values increased from 70 to 90 m²/g (Table 3). When the BET value approached 100 m²/g, about 35% of γ -Al₂O₃ in the powder system showed pseudomorph after boehmite (Table 3). It is known that the thermal treatment of the boehmite particles causes the release of structural water, which will initiate the exfoliation of boehmite particles. The exfoliation occurs only on the cleavage plane {010}_b, i.e., the planes of symmetry at the ends of the boehmite particles in the b-axis direction.

The generated γ -Al₂O₃ flakes showed a thickness of 5–6 nm with a slight shrink in size and preserved the appearance of boehmite (external form). This is significant because it causes the thinning of boehmite particles. Higher processing temperatures promote the appearance of γ -Al₂O₃ flakes. In addition, the increase in BET value and γ -Al₂O₃ content is accompanied by a decrease in meta- γ , indicating the energy input is crucial for the phase transformation and favors the formation of large-sized flakes.

3.3. Exfoliation Model

3.3.1. Two-Staged Procedures

The exfoliation process can be divided into two stages according to where the dominating operating forces originated from. The first stage occurred before the BET value reached $40 \text{ m}^2/\text{g}$. In the early stage of the phase transformation, the operating force came from the dehydration caused by the thermal treatments. The water vapor ejected from boehmite particles during dehydration broke the cleavage planes of the boehmite. This force dominated in the first-stage exfoliation. The second stage began when BET value was greater than $40 \text{ m}^2/\text{g}$. When the new phase $\gamma\text{-Al}_2\text{O}_3$ appeared, the strain due to shrinkage in dimension arising on the interface (cleavage plane) between the boehmite and $\gamma\text{-Al}_2\text{O}_3$ became an additional force. Therefore, in the second stage, both shrinkage strain and water vapor pressure coexisted, leading to the exfoliation.

3.3.2. Exfoliation Details

Stage One

As dehydration continued, boehmite vanished, and its content dropped to $\sim 70\%$. The meta- γ with a thickness of 6 nm was formed. The powder system consisted of boehmite and the newly formed meta- γ flakes, which are stripped from the cleavage planes $\{010\}_b$, the side pinacoid of the boehmite particle. In this stage, the average thickness of the boehmite particles was getting thinner, from 55 nm to 49 nm. When the BET value reached $40 \text{ m}^2/\text{g}$, the meta- γ content was about 30%, and the $\gamma\text{-Al}_2\text{O}_3$ flakes, which had been converted from meta- γ flakes, appeared. This is the end of the first stage of exfoliation.

Stage Two

In the second stage, $\gamma\text{-Al}_2\text{O}_3$ appeared, and the BET value exceeded $40 \text{ m}^2/\text{g}$. As the temperature further increased, the content of boehmite decreased and finally became null. The higher temperature favored the formation of meta- γ and its conversion to $\gamma\text{-Al}_2\text{O}_3$. The boehmite content continued to be decreased, and the average thickness decreased from 49 to 22 nm. The meta- γ flakes, as formed in the first stage, exfoliated from the side pinacoid of the boehmite particle and left the relics of boehmite. In addition, the formation and conversion rate of meta- γ accelerated, resulting in a high percentage of $\gamma\text{-Al}_2\text{O}_3$ formation and nearly absence of meta- γ . Finally, 2D alumina flake powders with a mean thickness of 5–6 nm were obtained while the BET value reached $\sim 100 \text{ m}^2/\text{g}$. Figure 8 illustrates the interpretation of the exfoliation model that occurred in this study.

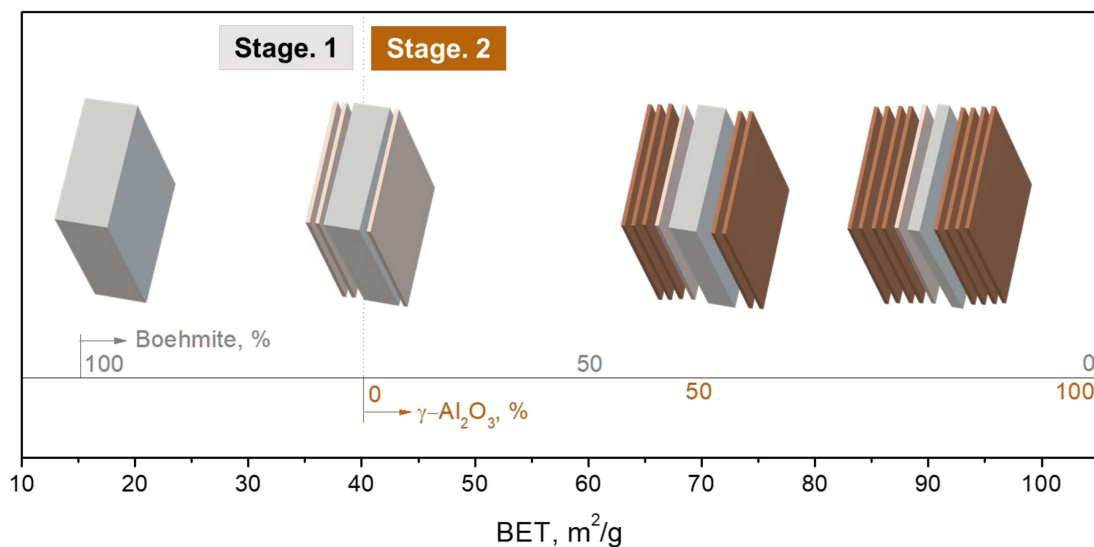


Figure 8. Schematic diagram of the powder exfoliation process at each stage.

3.3.3. Thermodynamics of the Flake Formation

Figure 4 demonstrates the TEM micrographs of the four types of flake particles observed in this study. It is interesting to note that all particles show similar morphology and obviously are the derivatives of boehmite $\{010\}_b$ cleavage planes. The calculated and measured thickness of the meta- γ and γ - Al_2O_3 flakes were 5–6 nm. Meanwhile, the final thickness of boehmite was 22 nm (calculated from BET value $\sim 90 \text{ m}^2/\text{g}$), which is close to 3 or 4 times 6 nm. The calculations in Table 4 show that the γ - Al_2O_3 particles with D_{50} of 450 nm and thickness of 5.7 nm and the boehmite particles with D_{50} of 450 nm and thickness of 22 nm have similar surface equivalent energies per unit flake (boehmite: $2.38 \times 10^{-10} \text{ mJ/flake}$, γ - Al_2O_3 : $5.05 \times 10^{-10} \text{ mJ/flake}$). This suggests that 2D powders can be generated in a natural way, cleaving or exfoliating during thermal treatment.

Table 4. Thermodynamics data.

| | Surface | Surface Area, | Surface Energy, | Energy/(Flake), |
|------------------------------------|---------|------------------------|---|------------------------|
| | | m^2 | mJ/m^2 | mJ |
| Boehmite | –10 | 3.18×10^{-13} | 455 ^{a,*,**} | 2.38×10^{-10} |
| | –101 | 3.11×10^{-14} | 4585 ^{a,*} –3000 ^{a,**} | |
| γ - Al_2O_3 | –110 | 3.18×10^{-13} | 2590 ^{b,*} –1540 ^{b,**} | 5.05×10^{-10} |
| | –111 | 8.06×10^{-15} | 4480 ^{b,*} –1970 ^{b,**} | |

^a Reference [59]. ^b Reference [60]. * Unrelaxed surface energy in vacuum. ** Relaxed surface energy in vacuum. (Adopted for calculation).

4. Conclusions

In summary, applying the thermal treatment to boehmite particles can produce exfoliation effects on it. Since boehmite exhibits perfect cleavage on the side pinacoid, $\{010\}$, by which boehmite has the potential to be stripped into flakes or exfoliation. In the thermal treatment, boehmite is transformed to γ - Al_2O_3 . The complete transformation process includes the dehydration and γ - Al_2O_3 formation, in which the water vapor pressure and shrink strain were induced, respectively. From the surface energy evaluations of boehmite and γ - Al_2O_3 and the results that the exfoliated flakes preserve the relics of boehmite, except for a reduced thickness of 5–6 nm (from the original 55 nm), it can be inferred that the exfoliation is a natural way of thermal treatment.

Author Contributions: Conceptualization, M.-Y.L. and F.-S.Y.; methodology, M.-Y.L.; software, M.-Y.L.; validation, M.-Y.L.; formal analysis, M.-Y.L.; investigation, M.-Y.L. and F.-S.Y.; resources, F.-S.Y. and H.-I.H.; data curation, M.-Y.L. and F.-S.Y.; writing—original draft preparation, M.-Y.L.; writing—review and editing, M.-Y.L.; F.-S.Y. and H.-I.H.; visualization, M.-Y.L.; supervision, F.-S.Y. and H.-I.H.; project administration, F.-S.Y. and H.-I.H.; funding acquisition, F.-S.Y. All authors have read and agreed to the published version of the manuscript.

Funding: This research was funded by LEATEC Fine Ceramics Co., Ltd. (project 110S068).

Data Availability Statement: Not applicable.

Acknowledgments: We would like to thank Ray from the Department of Resources Engineering at National Cheng-Kung University for providing many useful comments that helped to improve this study. We also extend our sincere appreciation to Wang and Wang at National Sun Yat-Sen University for serving as scientific advisors and data collection for FEGTEM (Tecnai F20 ID: EM0000011300) and Lee at National Cheng Kung University for data collection for AFM.

Conflicts of Interest: The authors declare no conflict of interest.

Appendix A. XRD Results Reveal the Phase Transformation during the Thermal Treatment

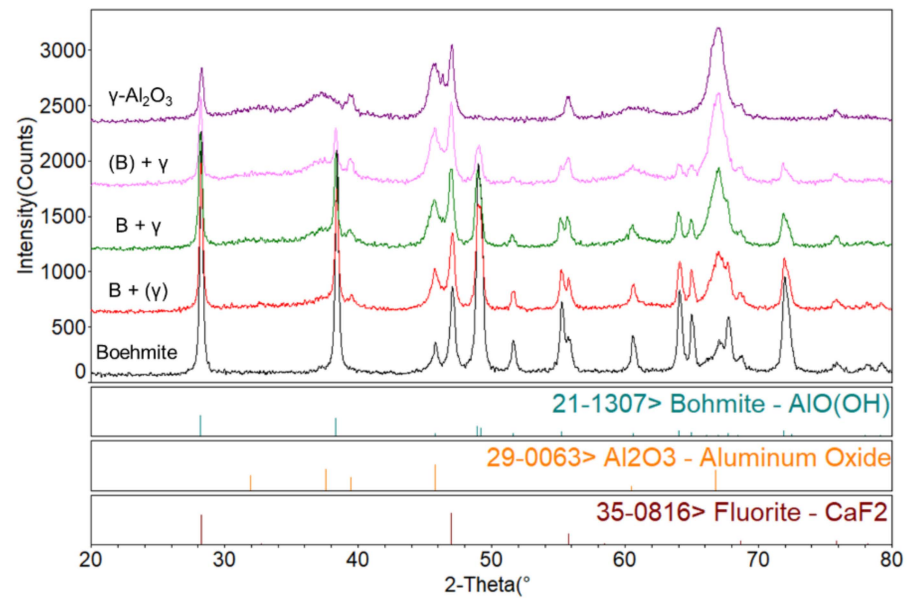


Figure A1. XRD qualitative analysis in phase transformation process.

Appendix B. Mean Thickness t_{BET} of the Calcined Boehmite/ γ - Al_2O_3 Flakes

This equation comes from two assumptions. First, the flake has a circular cross-sectional area with a diameter of D_{50} and thickness t . Second, all the newly generated surfaces increase in the direction of the cleavage plane. Therefore, the thickness t is related to the specific surface area value in this way.

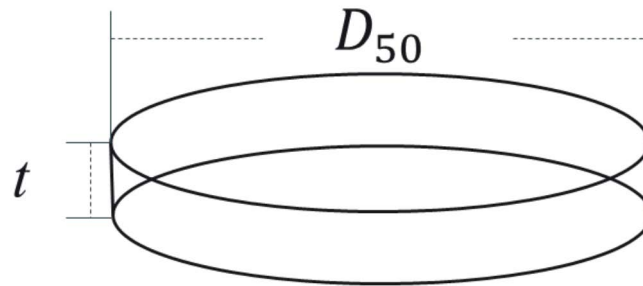


Figure A2. Schematic diagram of morphology assumptions for calculating the thickness of flake.

$$BET \text{ S.S.A. } \left(\frac{m^2}{g} \right) = \frac{\text{Surface area } (m^2)}{\text{Weight } (g)} = \frac{\frac{\pi \times D}{2} \times (D + 2t)}{W(g)} \quad (A1)$$

$$W(g) = \rho \times V = \rho \times \frac{\pi \times D^2}{4} \times t \quad (A2)$$

$$BET \text{ S.S.A.} = \frac{\frac{\pi \times D}{2} \times (D + 2t)}{\rho \times \frac{\pi \times D^2}{4} \times t} = \frac{2D + 4t}{\rho \times D \times t} = \frac{1}{\rho} \left(\frac{2}{t} + \frac{4}{D} \right) \quad (A3)$$

$$\rho \times BET \text{ S.S.A.} = \frac{2}{t} + \frac{4}{D} \quad \frac{1}{t} = \frac{\rho \times D \times BET \text{ S.S.A.} \times 10^{-3} - 4}{2D} \quad (A4)$$

$$\therefore t_{BET}(nm) = \frac{2D}{\rho \times D \times BET \text{ S.S.A.} \times 10^{-3} - 4} \quad (A5)$$

Appendix C. SAED Results of Boehmite/Meta- γ / γ -Al₂O₃

Table A1. Ratio of d values in the two directions of the cleavage plane obtained by SAED.

| | D-Spacing | | |
|--|-----------|-------|--------|
| | #1 | #2 | #1/#2 |
| Boehmite | 1.444 | 1.988 | 0.7264 |
| meta- γ | 1.443 | 2.003 | 0.7204 |
| γ -Al ₂ O ₃ | 1.431 | 2.002 | 0.7148 |

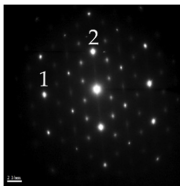
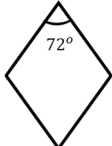
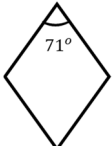


Table A2. SAED results and the associated morphology of boehmite and γ -Al₂O₃ in this study.

| Boehmite | | γ -Al ₂ O ₃ | | |
|--------------------|---|--|----------------------|---|
| a | 3.976 | → | 1/2 c γ | −4.004 |
| c | 2.888 | → | 1/2 d ₁₁₀ | −2.862 |
| {010} _b |  | | {110} γ |  |

References

- Tan, C.; Cao, X.; Wu, X.-J.; He, Q.; Yang, J.; Zhang, X.; Chen, J.; Zhao, W.; Han, S.; Nam, G.-H.; et al. Recent Advances in Ultrathin Two-Dimensional Nanomaterials. *Chem. Rev.* **2017**, *117*, 6225–6331. [[CrossRef](#)] [[PubMed](#)]
- Lin, Y.; Williams, T.; Connell, J.W. Soluble, Exfoliated Hexagonal Boron Nitride Nanosheets. *J. Phys. Chem. Lett.* **2009**, *1*, 277–283. [[CrossRef](#)]
- Fiori, G.; Bonaccorso, F.; Iannaccone, G.; Palacios, T.; Neumaier, D.; Seabaugh, A.; Banerjee, S.K.; Colombo, L. Electronics based on two-dimensional materials. *Nat. Nanotechnol.* **2014**, *9*, 768–779, Erratum in *Nat. Nanotechnol.* **2014**, *9*, 1063. [[CrossRef](#)] [[PubMed](#)]
- Wang, Q.H.; Kalantar-Zadeh, K.; Kis, A.; Coleman, J.N.; Strano, M.S. Electronics and optoelectronics of two-dimensional transition metal dichalcogenides. *Nat. Nanotechnol.* **2012**, *7*, 699–712. [[CrossRef](#)]
- Perez-Page, M.; Sahoo, M.; Holmes, S.M. Single Layer 2D Crystals for Electrochemical Applications of Ion Exchange Membranes and Hydrogen Evolution Catalysts. *Adv. Mater. Interfaces* **2019**, *6*. [[CrossRef](#)]
- Knözinger, H.; Ratnasamy, P. Catalytic Aluminas: Surface Models and Characterization of Surface Sites. *Catal. Rev.* **1978**, *17*, 31–70. [[CrossRef](#)]
- Wetzel, B.; Hauptert, F.; Friedrich, K.; Zhang, M.Q.; Rong, M.Z. Impact and wear resistance of polymer nanocomposites at low filler content. *Polym. Eng. Sci.* **2002**, *42*, 1919–1927. [[CrossRef](#)]
- Coleman, J.N.; Khan, U.; Blau, W.J.; Gun'Ko, Y.K. Small but strong: A review of the mechanical properties of carbon nanotube-polymer composites. *Carbon* **2006**, *44*, 1624–1652. [[CrossRef](#)]
- Novoselov, K.S.; Geim, A.K.; Morozov, S.V.; Jiang, D.; Zhang, Y.; Dubonos, S.V.; Grigorieva, I.V.; Firsov, A.A. Electric field effect in atomically thin carbon films. *Science* **2004**, *306*, 666–669. [[CrossRef](#)]
- Schniepp, H.C.; Li, J.-L.; McAllister, M.J.; Sai, H.; Herrera-Alonso, M.; Adamson, D.H.; Prud'Homme, R.K.; Car, R.; Saville, D.A.; Aksay, I.A. Functionalized Single Graphene Sheets Derived from Splitting Graphite Oxide. *J. Phys. Chem. B* **2006**, *110*, 8535–8539. [[CrossRef](#)]
- Wei, W.; Guan, T.; Li, C.; Shen, L.; Bao, N. Heating Rate-Controlled Thermal Exfoliation for Foldable Graphene Sponge. *Ind. Eng. Chem. Res.* **2020**, *59*, 2946–2952. [[CrossRef](#)]
- Mayorov, A.S.; Gorbachev, R.V.; Morozov, S.V.; Britnell, L.; Jalil, R.; Ponomarenko, L.A.; Blake, P.; Novoselov, K.S.; Watanabe, K.; Taniguchi, T.; et al. Micrometer-Scale Ballistic Transport in Encapsulated Graphene at Room Temperature. *Nano Lett.* **2011**, *11*, 2396–2399. [[CrossRef](#)]
- Geim, A.K.; Novoselov, K.S. The rise of graphene. In *Nanoscience and Technology*; World Scientific: Singapore, 2009; pp. 11–19.
- Pacile, D.; Meyer, J.; Girit, Ç.Ö.; Zettl, A. The two-dimensional phase of boron nitride: Few-atomic-layer sheets and suspended membranes. *Appl. Phys. Lett.* **2008**, *92*, 133107. [[CrossRef](#)]
- Alem, N.; Erni, R.; Kisielowski, C.; Rossell, M.D.; Gannett, W.; Zettl, A. Atomically thin hexagonal boron nitride probed by ultrahigh-resolution transmission electron microscopy. *Phys. Rev. B* **2009**, *80*, 155425. [[CrossRef](#)]
- Cui, Z.; Oyer, A.J.; Glover, A.J.; Schniepp, H.C.; Adamson, D.H. Large Scale Thermal Exfoliation and Functionalization of Boron Nitride. *Small* **2014**, *10*, 2352–2355. [[CrossRef](#)]
- Li, H.; Wu, J.; Yin, Z.; Zhang, H. Preparation and Applications of Mechanically Exfoliated Single-Layer and Multilayer MoS₂ and WSe₂ Nanosheets. *Accounts Chem. Res.* **2014**, *47*, 1067–1075. [[CrossRef](#)]

18. Li, L.; Zhang, D.; Gao, Y.; Deng, J.; Gou, Y.; Fang, J. Electric field driven exfoliation of MoS₂. *J. Alloy. Compd.* **2021**, *862*, 158551. [[CrossRef](#)]
19. Li, M.-Y.; Shi, Y.; Cheng, C.-C.; Lu, L.-S.; Lin, Y.-C.; Tang, H.-L.; Tsai, M.-L.; Chu, C.-W.; Wei, K.-H.; He, J.-H.; et al. Epitaxial growth of a monolayer WSe₂-MoS₂ lateral p-n junction with an atomically sharp interface. *Science* **2015**, *349*, 524–528. [[CrossRef](#)]
20. Gerstner, E. Nobel Prize 2010: Andre Geim & Konstantin Novoselov. *Nat. Phys.* **2010**, *6*, 836. [[CrossRef](#)]
21. Novoselov, K.S.; Jiang, D.; Schedin, F.; Booth, T.J.; Khotkevich, V.V.; Morozov, S.V.; Geim, A.K. Two-dimensional atomic crystals. *Proc. Natl. Acad. Sci. USA* **2005**, *102*, 10451–10453. [[CrossRef](#)]
22. Ciesielski, A.; Samorì, P. Graphene via sonication assisted liquid-phase exfoliation. *Chem. Soc. Rev.* **2014**, *43*, 381–398. [[CrossRef](#)] [[PubMed](#)]
23. Coleman, J.N. Liquid-Phase Exfoliation of Nanotubes and Graphene. *Adv. Funct. Mater.* **2009**, *19*, 3680–3695. [[CrossRef](#)]
24. Agrawal, A.; Yi, G.-C. Sample pretreatment with graphene materials. *Compr. Anal. Chem.* **2020**, *91*, 21–47. [[CrossRef](#)]
25. Nagyte, V.; Kelly, D.J.; Felten, A.; Picardi, G.; Shin, Y.; Alieva, A.; Worsley, R.E.; Parvez, K.; Dehm, S.; Krupke, R.; et al. Raman Fingerprints of Graphene Produced by Anodic Electrochemical Exfoliation. *Nano Lett.* **2020**, *20*, 3411–3419. [[CrossRef](#)]
26. Dileep, N.P.; Vineesh, T.V.; Sarma, P.V.; Chalil, M.V.; Prasad, C.S.; Shaijumon, M.M. Electrochemically Exfoliated β -Co(OH)₂ Nanostructures for Enhanced Oxygen Evolution Electrocatalysis. *ACS Appl. Energy Mater.* **2020**, *3*, 1461–1467. [[CrossRef](#)]
27. Zhang, H.-B.; Wang, J.-W.; Yan, Q.; Zheng, W.-G.; Chen, C.; Yu, Z.-Z. Vacuum-assisted synthesis of graphene from thermal exfoliation and reduction of graphite oxide. *J. Mater. Chem.* **2011**, *21*, 5392–5397. [[CrossRef](#)]
28. Botas, C.; Álvarez, P.; Blanco, C.; Santamaria, R.; Granda, M.; Gutiérrez, M.D.; Rodriguez-Reinoso, F.; Menéndez, R. Critical temperatures in the synthesis of graphene-like materials by thermal exfoliation–reduction of graphite oxide. *Carbon* **2013**, *52*, 476–485. [[CrossRef](#)]
29. Tan, C.; Zhang, H. Wet-chemical synthesis and applications of non-layer structured two-dimensional nanomaterials. *Nat. Commun.* **2015**, *6*, 7873. [[CrossRef](#)]
30. Sun, Z.; Liao, T.; Dou, Y.; Hwang, S.M.; Park, M.-S.; Jiang, L.; Kim, J.H.; Dou, S.X. Generalized self-assembly of scalable two-dimensional transition metal oxide nanosheets. *Nat. Commun.* **2014**, *5*, 3813. [[CrossRef](#)]
31. Sun, Y.; Sun, Z.; Gao, S.; Cheng, H.; Liu, Q.; Piao, J.; Yao, T.; Wu, C.; Hu, S.; Wei, S.; et al. Fabrication of flexible and freestanding zinc chalcogenide single layers. *Nat. Commun.* **2012**, *3*, 1057. [[CrossRef](#)]
32. Lee, Y.-H.; Zhang, X.-Q.; Zhang, W.; Chang, M.-T.; Lin, C.-T.; Chang, K.-D.; Yu, Y.-C.; Wang, J.T.-W.; Chang, C.-S.; Li, L.-J.; et al. Synthesis of Large-Area MoS₂ Atomic Layers with Chemical Vapor Deposition. *Adv. Mater.* **2012**, *24*, 2320–2325. [[CrossRef](#)]
33. Ji, Q.; Zhang, Y.; Zhang, Y.; Liu, Z. Chemical vapour deposition of group-VIB metal dichalcogenide monolayers: Engineered substrates from amorphous to single crystalline. *Chem. Soc. Rev.* **2014**, *44*, 2587–2602. [[CrossRef](#)]
34. Mahler, B.; Hoepfner, V.; Liao, K.; Ozin, G.A. Colloidal Synthesis of 1T-WS₂ and 2H-WS₂ Nanosheets: Applications for Photocatalytic Hydrogen Evolution. *J. Am. Chem. Soc.* **2014**, *136*, 14121–14127. [[CrossRef](#)]
35. Yin, A.-X.; Liu, W.-C.; Ke, J.; Zhu, W.; Gu, J.; Zhang, Y.-W.; Yan, C.-H. Ru Nanocrystals with Shape-Dependent Surface-Enhanced Raman Spectra and Catalytic Properties: Controlled Synthesis and DFT Calculations. *J. Am. Chem. Soc.* **2012**, *134*, 20479–20489. [[CrossRef](#)]
36. Yin, X.-L.; Li, L.-L.; Jiang, W.-J.; Zhang, Y.; Zhang, X.; Wan, L.-J.; Hu, J.-S. MoS₂/CdS Nanosheets-on-Nanorod Heterostructure for Highly Efficient Photocatalytic H₂ Generation under Visible Light Irradiation. *ACS Appl. Mater. Interfaces* **2016**, *8*, 15258–15266. [[CrossRef](#)]
37. Bowles, J.F.W. Hydroxides. In *Encyclopedia of Geology (Second Edition)*; Alderton, D., Elias, S.A., Eds.; Academic Press: Oxford, UK, 2021; Volume 1, pp. 442–451.
38. Wefers, K.; Misra, C. *Oxides and Hydroxides of Aluminum*; Alcoa Laboratories: Pittsburgh, PA, USA, 1987; Volume 19.
39. Wilson, S. The dehydration of boehmite, γ -AlOOH, to γ -Al₂O₃. *J. Solid State Chem.* **1979**, *30*, 247–255. [[CrossRef](#)]
40. Wilson, S.; Mc Connell, J. A kinetic study of the system γ -AlOOH/Al₂O₃. *J. Solid State Chem.* **1980**, *34*, 315–322. [[CrossRef](#)]
41. Tsuchida, T.; Furuichi, R.; Ishii, T. Kinetics of the dehydration of boehmites prepared under different hydrothermal conditions. *Thermochim. Acta* **1980**, *39*, 103–115. [[CrossRef](#)]
42. Volpe, L.; Boudart, M. Topotactic Preparation of Powders with High Specific Surface Area. *Catal. Rev.* **1985**, *27*, 515–538. [[CrossRef](#)]
43. Tertian, R.; Papée, D. Transformations thermiques et hydrothermiques de l’alumine. *J. Chim. Phys.* **1958**, *55*, 341–353. [[CrossRef](#)]
44. De Boer, J.H.; Fortuin, J.M.H.; Steggerda, J.J. The dehydration of alumina hydrates. *Proc. K. Ned. Akad. Wet. B* **1954**, *57*, 170–180.
45. Gitzen, W.H. *Alumina as a Ceramic Material*; American Ceramic Society: Columbus, OH, USA, 1970.
46. Hart, L.R.D.; Lense, E. *Alumina Chemicals: Science and Technology Handbook*; The American Ceramic Society: Westerville, OH, USA, 1990.
47. Van Gog, H. First-principles study of dehydration interfaces between diaspore and corundum, gibbsite and boehmite, and boehmite and γ -Al₂O₃: Energetic stability, interface charge effects, and dehydration defects. *Appl. Surf. Sci.* **2020**, *541*, 148501. [[CrossRef](#)]
48. Gates-Rector, S.; Blanton, T. The Powder Diffraction File: A quality materials characterization database. *Powder Diffr.* **2019**, *34*, 352–360. [[CrossRef](#)]
49. Kim, D.; Jung, J.H.; Ihm, J. Theoretical Study of Aluminum Hydroxide as a Hydrogen-Bonded Layered Material. *Nanomaterials* **2018**, *8*, 375. [[CrossRef](#)]

50. Conroy, M.; Soltis, J.A.; Wittman, R.S.; Smith, F.N.; Chatterjee, S.; Zhang, X.; Ilton, E.S.; Buck, E.C. Importance of interlayer H bonding structure to the stability of layered minerals. *Sci. Rep.* **2017**, *7*, 13274. [[CrossRef](#)]
51. Yang, Y.; Zhong, Y.; Wang, X.; Ma, Y.; Yao, J. Facile Synthesis of Ultrathin Lepidocrocite Nanosheets from Layered Precursors. *Chem. Asian J.* **2014**, *9*, 1563–1569. [[CrossRef](#)]
52. McAteer, D.; Godwin, I.J.; Ling, Z.; Harvey, A.; He, L.; Boland, C.S.; Vega-Mayoral, V.; Szydłowska, B.; Rovetta, A.A.; Backes, C.; et al. Liquid Exfoliated Co(OH)₂ Nanosheets as Low-Cost, Yet High-Performance, Catalysts for the Oxygen Evolution Reaction. *Adv. Energy Mater.* **2018**, *8*, 1702965. [[CrossRef](#)]
53. Schmidt, M.; Lutz, H. γ -Cd(OH)₂, a common hydroxide or an aquoxy-hydroxide? *Mater. Res. Bull.* **1991**, *26*, 605–612. [[CrossRef](#)]
54. Nonat, A.; Mutin, J. Evolution des dimensions des cristallites des phases initiale et finale au cours de la deshydratation mecanique: Cd(OH)₂ → CdO + H₂O. *Mater. Chem.* **1982**, *7*, 479–498. [[CrossRef](#)]
55. Lowell, S.; Shields, J.E. The single point BET method. In *Powder Surface Area and Porosity*; Springer: Dordrecht, The Netherlands, 1984; pp. 30–35. [[CrossRef](#)]
56. Walton, W.H. Feret's Statistical Diameter as a Measure of Particle Size. *Nature* **1948**, *162*, 329–330. [[CrossRef](#)]
57. Holzwarth, U.; Gibson, N. The Scherrer equation versus the 'Debye-Scherrer equation'. *Nat. Nanotechnol.* **2011**, *6*, 534. [[CrossRef](#)]
58. Krokidis, X.; Raybaud, P.; Gobichon, A.-E.; Rebours, B.; Euzen, P.; Toulhoat, H. Theoretical Study of the Dehydration Process of Boehmite to γ -Alumina. *J. Phys. Chem. B* **2001**, *105*, 5121–5130. [[CrossRef](#)]
59. Digne, M. Use of DFT to achieve a rational understanding of acid/basic properties of γ -alumina surfaces. *J. Catal.* **2004**, *226*, 54–68. [[CrossRef](#)]
60. Raybaud, P.; Digne, M.; Iftimie, R.; Wellens, W.; Euzen, P.; Toulhoat, H. Morphology and Surface Properties of Boehmite (γ -AlOOH): A Density Functional Theory Study. *J. Catal.* **2001**, *201*, 236–246. [[CrossRef](#)]